Submitted to: Remote Sensing of Environment (RSE)

Continuous and long-term measurements of reflectance and sun-induced chlorophyll fluorescence by using novel automated field spectroscopy systems

S. Cogliati[a,], M. Rossini[a], T. Julitta[a], M. Meroni[a,b], A. Schickling[c], A. Burkart[c], F. Pinto[c], U. Rascher[c], R. Colombo[a]*

[a] *Remote Sensing of Environmental Dynamics Lab., DISAT, University of Milan-Bicocca, P.zza della Scienza 1, 20126, Milan, Italy;*

[b] *European Commission, Joint Research Centre (JRC), Institute for Environment and Sustainability (IES), Monitoring Agricultural Resources Unit, Via Fermi 2749, Ispra, Italy;*

[c] *Institute of Bio- and Geosciences, IBG-2: Plant Sciences, Forschungszentrum Jülich GmbH, Leo-Brandt-Str., 52425 Jülich, Germany.*

Keywords: proximal sensing, automated field spectroscopy systems, hyperspectral missions, calibration/validation, Sun-Induced Fluorescence, FLEX.

***Corresponding author**: sergio.cogliati@unimib.it, +39-0264482860, Remote Sensing of Environmental Dynamics Lab., University of Milan-Bicocca, P.zza della Scienza 1, 20126, Milan, Italy

Abstract

In this paper we present novel automated field spectroscopy systems for collecting unattended, continuous and long-term measurements of plant canopies and, more in general, of Earth's ecosystems. These systems simultaneously collect *high* and *ultra-high* resolution spectra in the visible to near-infrared (VNIR) domain employing two spectrometers: i) the first covers the spectral range 400-1000 nm with a 1.0 nm spectral resolution; ii) the second provides a sub-nanometer spectral resolution within the 700-800 nm spectral range. The data collected by the first spectrometer allow retrieval of VNIR reflectance, while the higher spectral resolution data from the second device permit estimation of vegetation Sun-Induced Fluorescence (SIF) in the O_2-A band. The instruments are constructed by assembling commercial and on-the-shelf optoelectronic devices to facilitate reproduction of the instrument for promoting measurements over different ecosystems. The instrument's optical design, data collection and processing, laboratory and in-field calibration methods are reported and discussed. The high spectral resolution and the rigorous calibration methods enable accurate estimation of SIF in physical units by exploiting almost the same retrieval concept as that of the European Space Agency FLuorescence EXplorer mission. The instruments have been operated in several field campaigns with the aim to show: i) the possibility of continuous and seasonal monitoring of plant growth and activity of an agricultural crop; and ii) the diverse and specific daily course patterns of different types of canopy. The datasets of canopy reflectance, vegetation indices and sun-induced fluorescence collected are shown and discussed.

1 Introduction

Hyperspectral remote sensing is becoming a powerful and reliable approach for Earth observations, as it allows a detailed observation of important bio- and geo-physical parameters related to Earth's dynamic processes. The use of hyperspectral sensors has various advantages (Goetz, 2009) including: i) detection of narrow spectral features related to particular parameters; ii) exploitation of over-determined mathematical equations to increase the retrieval accuracy; and iii) simultaneous estimation of a certain number of parameters. The benefits of hyperspectral data have been demonstrated for many environmental applications covering studies on the biosphere, atmosphere, cryosphere, lithosphere and hydrosphere (Schaepman et al., 2009).

Currently, the Hyperion sensor launched by NASA in November 2000 aboard the Earth Observing-1 (Middleton et al., 2013; Ungar et al., 2003) is still the only hyperspectral satellite mission devoted to land surface studies. In the last decade, several studies have laid the basis for upcoming space missions for supplying operational hyperspectral observations of Earth-surface reflected radiance. The Hyperspectral Infrared Imager (HyspIRI) (Green et al., 2008) under development by NASA, the Environmental Mapping and Analysis Program (EnMAP) (Kaufmann et al., 2008) by the German Aerospace Center (DLR) and the Hyperspectral Precursor of the Application Mission (PRISMA) (Galeazzi et al., 2009) by the Italian Space Agency (ASI), are some of the programs that will be launched in the next few years.

Beyond these, the FLuorescence EXplorer (FLEX) mission currently candidate to the European Space Agency (ESA) 8^{th} Earth Explorer (EE8) (Drusch et al., 2008) aims to detect the faint red glow of the Sun-Induced Fluorescence signal (SIF) emitted by plants. The FLEX satellite carries the FLuORescence Imaging Spectrometer (FLORIS) (Kraft et al., 2013; Kraft, 2012) to measure fluorescence at the oxygen absorption bands, the reflectance in the red-edge and the Photochemical Reflectance Index (PRI). It will fly in tandem with the Sentinel-3 satellite to take advantage of complementary measurements from the Ocean and Land Color Instrument (OLCI) and the Sea and Land Surface Temperature Radiometer (SLSTR).

The exploitation of the SIF signal is a novel approach to inferring plants' photosynthetic activity improving vegetation gross primary production models of natural and managed ecosystems (Baker, 2008; Flexas et al., 2002; Papageorgiou & Govindjee, 2004). In fact, plants respond continuously to the varying environmental conditions that modulate the photosynthetic rate. The SIF signal is promising as a probe of this process because it arises directly from the core of the photosynthetic machinery, thus providing instantaneous information on plant functioning (Damm et al., 2012; Zarco-Tejada et al., 2009, 2013).

In support of future satellite missions, airborne and field spectroscopy measurements have a fundamental role, offering valuable data to consolidate instrument's features, algorithm prototyping and to better understand the link between optical signals and parameters/processes at different observational scales. Recently, in support of FLEX preparatory studies, the novel high-performance airborne imaging spectrometer *HyPlant* and ground-based high-resolution spectroscopy systems have been developed and operated during extensive field campaigns to study the spatial and temporal behaviors of SIF. The *HyPlant* is a narrow-band imaging spectrometer developed by the Forschungszentrum Jülich (Jülich Research Center, Germany) in cooperation with SPECIM Imaging Ltd. (Finland). The imagery provided by *HyPlant* (Rossini et al., 2015) was fundamental in retrieving the first airborne maps of SIF at high spatial resolution (1-3 m) and investigating the contributions of the different landscape elements to the upwelling signal. In parallel, ground-based instruments provide ground-truth measurements for remote sensing data, and furthermore they are powerful tools in investigating the temporal (i.e. diurnal to seasonal) behavior of SIF in relation to plant photosynthesis. In the last decade, automatic field spectroradiometers for unattended measurements of vegetation by using different instruments and configurations (Corp et al., 2010; Daumard et al., 2010; Drolet et al., 2014; Gamon et al., 2006; Hilker et al., 2010; Huber et al., 2014; Leuning et al., 2006; Meroni et al., 2011) have been proposed. A review of some of the instruments employed for continuous vegetation optical sampling in flux towers sites is available from Balzarolo et al. (2011). Most of these instruments offer spectral measurements in the visible to near-infrared (VNIR), but the only ones featuring high-resolution spectrometers for SIF detection are those proposed in Meroni et al., (2011) and Daumard et al., (2010). In this framework, the international initiatives SpecNet (Gamon et al., 2006), the ESSEM COST action EUROSPEC (ES0903) and the recently founded ESSEM COST action OPTIMISE (ES1309) aim at the definition of common ground-based instruments, measurement protocols and data processing as the basis for a further global network. The distributed and systematic/standardized ground-based measurements within the network will potentially offer several advantages to the remote sensing community for improving atmospheric corrections, calibration/validation of airborne and satellite products and understanding optical signals in both space and time domains.

In this paper, we present two automated field spectroscopy systems, the Multiplexer Radiometer Irradiometer (MRI) and its compacted version SFLUOR box, which are capable of collecting unattended, continuous, long-term hyperspectral measurements. The instruments' technical design, the rigorous calibration methods, the data collection, and processing chain are explained through the paper. The reliability of radiance, reflectance, and derived spectral indices collected in different remote sensing campaigns are presented and discussed. In particular, the possibility of continuous and long-term monitoring of plant growth and activity is evaluated during the entire growing season of an agricultural crop. Thereafter, extensive ground-based measurements collected for the calibration and validation of the *HyPlant* sensor, allowed to observe the diverse and specific daily course patterns of different types of canopy. Although the use of these instruments is mainly intended for vegetation studies, spectral measurements collected may be helpful in studying the temporal dynamics over any terrestrial ecosystem (e.g. inland water, snow, glaciers, and soils), and they can support calibration and validation of airborne and satellite remote sensing data.

2 Instruments description

The automated field spectroscopy systems were developed by assembling commercial-grade optoelectronic devices. The design concept is based on the use of an optical switch to sequentially select between several input fiber optics fixed to the up-looking (i.e. toward zenith) and the down-looking entrance foreoptic. The optical switch is a fiber optics multiplexer MPM-2000-2x8-VIS (Ocean Optics Inc., USA) with optical throughput >40% in the VNIR (350-1000 nm) able to connect up to 8 different input channels to output ports connected to two different spectrometers. The switch between adjacent input channels is performed in 150 ms with a positioning accuracy above 99% using a direct current motor with encoder. The actual configuration connects each spectrometer to 3 input ports: i) the up-looking CC-3 cosine-corrected irradiance probes (Ocean Optics Inc., USA) to collect the down-welling irradiance (E_g); ii) the down-looking bare fiber optics with a Field-of-View (FOV) of 25° to measure the up-welling radiance from the target surface (L_s) and; iii) a “blind” port used to record the instrument dark-current (DC). The conceptual layout of the instruments is shown in Figure 1A. The entrance foreoptics are connected to the multiplexer input ports using 5 m long optical fibers (one for each spectrometer) with a bundle core of 1000 μm diameter. The connection between the multiplexer output ports and the spectrometers is obtained with 0.3 m long optical fibers. This set-up enables sequential measurements of DC, E_g and L_s spectra simultaneously with two spectrometers.

<Figure 1>

The two spectrometers embedded in these systems are the High-Resolution HR4000 holographic grating spectrometers (Ocean Optics Inc., USA) covering the VNIR with different spectral resolutions. The first spectrometer (hereafter $SPEC_{Full}$) covers the 400-1000 nm spectral range with a *Full Width at Half Maximum* (FWHM) ≃ 1.0 nm. The second spectrometer (hereafter $SPEC_{Fluo}$) is instead optimized to provide higher spectral resolution (FWHM ≃ 0.1 nm) in the 700-800 nm range around the atmospheric oxygen absorption band at 760 nm (O_2-A). The spectrometer optical bench consists of a 5μ*m* wide entrance slit, diffraction grating with a groove density of 600 (1800) mm^{-1} for $SPEC_{Full}$ ($SPEC_{Fluo}$) respectively and the 3648-element linear CCD-array detector (Toshiba TCD1304AP, Japan) with a 14-bit A/D resolution. Currently, commercial linear CCD detectors offer a relatively limited number of pixels over the spectrum at the different wavelengths. Therefore, the integration of two spectrometers into the MRI system was required to provide both the high spectral resolution for fluorescence retrieval and the continuous VNIR spectral coverage at the same time. The main technical characteristics of the HR4000 spectrometers are summarized in Table 1.

<Table 1>

The devices embedded in the field spectroscopy systems are connected to a PC that controls the multiplexer via RS232 and the spectrometers through a USB 2.0 connection. The multiplexer, spectrometers and electronic devices are hosted in a waterproof box customized to permit connection to the optics and electrical interfaces. A cooling system limits variations of the box air temperature thus reducing instrument-related effects such as spectral drifts and detector noise.

The MRI and SFLUOR box have the same optical design concept and operative procedures. However, the SFLUOR box was built recently; therefore, minor technical solutions were improved based on the previous experience. The SFLUOR box differs for an overall compact design (box dimensions 0.31 m × 0.55 m × 0.48 m), and for the integration of the cooling system within the instrument box. These technical solutions facilitate the field installation of the instrument, especially when it must be operated on scaffolding towers to perform measurements over forest canopies. A typical example of the installation of MRI and SFLUOR box in the field for continuous measurements is shown in Figure 1B and C, respectively.

2.1 Field Spectroscopy technique and Data Collection

Determination of canopy reflectance and fluorescence from field spectroscopy measurements relies on measurements of E_g and L_s radiances with the assumption of constant illumination conditions and surface anisotropy (Eq 1).

$$L_s(\lambda) = \rho(\lambda)\frac{E_g(\lambda)}{\pi} + SIF(\lambda) \qquad \text{Eq. 1}$$

The ρ is the canopy reflectance and E_g is the integral of incoming radiance over the hemisphere (i.e. direct/diffuse radiances). Since the optical path between the sensor and the target surface is limited to a few meters during field spectroscopy measurements and is held constant, the influence of the atmosphere in the path between target and sensor is neglected.

According to Schaepman-Strub et al. 2006, the ratio of L_s and E_g spectra as collected by MRI and SFLUOR box is formally referred to as the Hemispherical-Conical Reflectance Factor (HCRF). However, the reference nomenclature does not account for SIF contribution in the case of measurements collected over vegetation. In fact, the term L_s (Eq 1) includes both the canopy reflected radiance and SIF contributions; therefore, the "apparent" reflectance, ρ* (Eq 2), is introduced (Alonso et al., 2008; Meroni & Colombo, 2006) to distinguish it from the reflectance term free of fluorescence.

$$\rho^*(\lambda) = \frac{\pi\, L_s(\lambda)}{E_g(\lambda)} \qquad \text{Eq. 2}$$

The custom-developed software Auto3S synchronizes instrument's operations to control the MPM-2000 and to manage the spectrometer settings and spectra collection. This software is the automatic version of the 3S program previously developed by Meroni & Colombo (2009) for manual acquisition of field spectroscopy measurements. The data acquisition program is developed in the LabWindows/CVI Instruments 2010 environment and compiled into an executable file to run under Microsoft Windows operating systems. The software application uses the libraries provided with the driver OOI-WinIP (OOIDrv32.lib, Ocean Optics Inc., USA) to control the HR4000 spectrometers and the RS232 serial protocol to switch between the different channels of MPM-2000.

Spectra acquisition follows the *Single Beam Sandwiched* method suggested in Meroni et al. (2008). The methodology consists of the sequential measurement of the incoming irradiance ($E_{g,1}$), the up-welling radiance from the target surface (L_s) and a second irradiance measurement ($E_{g,2}$). The down-welling irradiance at the time of sample acquisition, E_g, is estimated by linear interpolation of $E_{g,1}$ and $E_{g,2}$ at the time of sample acquisition. This approach is helpful in adjusting small monotonic variations of incident radiation intensity during a single acquisition session (i.e. between $E_{g,1}$, L_s and $E_{g,2}$ measurements) that may occur due to small variations in sun position (i.e. particularly in the morning/afternoon) or due to slight changes in atmospheric conditions.

The data collection scheme also includes optimization (*Opt*) of spectrometer integration time (*IT*) and measurement of instrument DC. The *IT* determines the amount of energy that reaches the sensor and is generally chosen to maximize the usage of the full dynamic range with the aim of maximizing the Signal to Noise Ratio (SNR) as well. The IT is set automatically at the beginning of each acquisition session to evaluate Eq. 3 iteratively until the optimal value is reached. The latter is defined as the one ensuring that the maximum intensity of the spectrum falls in the range comprised between pre-defined lower and upper limits (i.e. 85-95%) of the spectrometer saturation value (sv). The use of a range of optimal values makes it possible to satisfy Eq 3 earlier than with the use of a single scalar value.

$$IT_{i+1} = IT_i \frac{Opt}{peak_i} k \qquad \text{Eq. 3}$$

The IT_{i+1} is the new *IT* optimized for the new acquisition session; IT_i is the *IT* of the previous measurement session; $peak_i$ is the average of 10 spectral bands expressed in digital counts at the maximum of the current spectrum recorded; and *Opt* the corresponding optimal value of the signal, defined as the mean value between the lower and upper limits. The $peak_i$ values collected at different ITs during the algorithm iterations are not corrected for the corresponding DC, thus reducing the time needed for the execution of the algorithm. The relative contribution of DC to the total signal is not linearly related to IT because this contribution is lower at higher integration time. Therefore, the optimal value of the IT cannot be reached in a single step and one more iteration is needed. The k correction coefficient, estimated empirically from measurements at the different ITs (k=1.15), is introduced to achieve optimal IT within a single iteration. The algorithm-based selection of the optimal *IT* may fail when sky conditions are extremely variable (e.g. partly cloudy). In these cases, if the iterative search of the *IT* cannot be concluded within a predefined time limit (i.e. 60 s), the measurement session is aborted and the event traced into the log file. The log file is updated with any event connected with software or hardware failures that preclude normal completion of the measurement cycle. The typical IT values during a cloud-free day at mid latitudes around noon (early morning) are about of 0.2 s (1 s) for the $SPEC_{Full}$ and 0.7 s (1.8 s) $SPEC_{Fluo}$. By default, a number of 10 and 4 scans for $SPEC_{Full}$ and $SPEC_{Fluo}$ respectively are internally averaged by the spectrometers and subsequently stored on the controller pc hard drive as a binary file. The single acquisition session is initialized systematically with a predefined time step (every 3-5 minutes) which permits completion of the entire sequence of measurements.

The MRI and SFLUOR box up-looking and down-looking optical channels present different optical throughput, lower for the cosine-receptor foreoptic as compared to the bare fiber. As a result, the energy reaching the sensor when measuring L_s can be greater than E_g. This uncertainty requires an adaptation of the IT optimization procedure, normally performed on the incident irradiance in field spectroscopy operations. Specifically, Auto3S includes three different optimization methods to prevent the saturation of both the signals: i) the optimization of the up-looking channel for measurements over dark surfaces (when $E_g >> L_s$); ii) the optimization of the down-looking channel for measurements over bright surfaces (when $L_s >> E_g$); iii) the optimization of both channels.

The first two operational modes (i.e. single-channel) can be used when the relative magnitude of the two signals is known. They have the advantage of being faster because the *IT* optimization algorithm is launched only once. On the contrary, the third approach (i.e. dual-channel) requires performing the optimization twice, but it has the advantage of preventing saturation of both E_g and L_s measurements for any surface and illumination conditions. Moreover, it allows maintaining the SNR level as high as possible to exploit a larger spectrometer dynamic range. The latter mode is typically used when the instruments are left unattended for a long time period in which surface reflectance may change (e.g. a crop cycle with a surface ranging from bare soil to fully closed canopy). The detailed flow-chart of the steps carried out by Auto3S to complete a single acquisition session when the single and the dual-channel optimization methods are selected are reported in Figure 2.

<Figure 2>

2.2 Spectral and Radiometric calibration

The accurate characterization and calibration to traceable international standards (e.g. US National Institute of Standards and Technology, NIST) is mandatory to provide accurate radiance and reflectance data. A regular calibration is particularly relevant for instruments aimed at long-term data collection operated outdoors and continuously exposed to varying environmental factors that affect instrument performance and cause aging and/or degradation of the sensor (i.e. temperature, rain, humidity, dust etc.). Furthermore, recent applications, such as detection of SIF, rely on the analysis of very narrow absorption features and this makes instrument stability and precise characterization of the response fundamental for accurate detection of the signal (Damm et al., 2011; Guanter et al., 2009).

Well-established laboratory calibration methods must be performed regularly are not functional to be conducted regularly in-field to assure high data quality levels. For this reason, traditional methods are combined with in-field vicarious techniques for completing a regular check of instrument calibration factors.

Laboratory spectral calibration is achieved by applying an improved version of the standard methodology proposed by the spectrometer manufacturer (Ocean Optics Inc., USA). The lines emitted in the VNIR range (250-920 nm) by the light calibration source (CAL-2000 Mercury Argon Lamp; Ocean Optics Inc., US) are used. The band center and FWHM are retrieved by modeling the detected emission lines by least square fitting of gaussian/lorentzian functions. The wavelength (λ) vector is calculated by least square fitting of a 3rd degree polynomial function that refers the theoretical wavelength to the pixel number where lines are detected. However, the band center positions and FWHMs may slightly drift due to the aging and degradation of the optical system, misalignment due to mechanical shocks and variations induced by environmental factors (Gao et al., 2004; Guanter et al., 2006, 2009). A spectrum matching technique named SpecCal developed by Meroni et al. (2010) is used as vicarious calibration to routinely check spectral shift (SS) and FWHM by comparing spectra collected by MRI against theoretical spectra modeled with the MODTRAN5 radiative transfer code (Berk et al., 2006) in selected spectral windows characterized by strong absorption features.

Absolute radiometric calibration is carried out in the laboratory using a NIST-traceable HL-2000-CAL Calibrated Tungsten Halogen Light Source (Ocean Optics Inc., USA) and in the field by cross-calibration against a laboratory-calibrated reference spectrometer. The nonlinear behavior is characterized and corrected by following the methodology proposed by the spectrometer's manufacturer. In-field radiometric cross-calibration measurements are collected by exploiting the following set-up: a standard white reference panel (Optopolymer GmbH, Germany) is placed in the FOV of MRI and SFLUOR box down-looking channel and simultaneous measurements of the same panel are acquired with a reference calibrated spectrometer. In this way, nearly contemporary spectra of E_g are collected by: i) the cosine-receptor (up-looking channel); ii) the bare fiber optics (down-looking channel); and iii) reference spectrometer. The measurements are repeated throughout daylight hours (i.e. different solar zenith angles, SZA) thus reducing the dependence on light intensities and angular distributions. The spectra are convolved to the bands of the reference instrument and gain factors $g(\lambda)$ are deduced by comparing reference radiance values with digital counts recorded by MRI and SFLUOR box employing Eq. 4. This approach allows regular updating of the radiometric calibration coefficients without the need to take the instrument to in-house calibration facilities.

$$L_s(\lambda) = \frac{Counts(\lambda) - DC(\lambda)}{IT}\, g(\lambda) \qquad \text{Eq. 4}$$

The L_s is the radiance recorded by the reference spectrometer, Counts are the raw digital counts from the MRI and SFLUOR box to be calibrated, *IT* is the integration time used for each measurements and *g* the gains factor at different wavelengths.

3 Data processing

3.1 Basic processes and Data Quality

The processing of the large amounts of spectra collected by the automated systems is carried out with a computer code developed in IDL 8.2.0 (Exelis Visual Information Solutions, USA) programming language. The processing chain includes a series of operations to convert instrument digital counts to radiance in physical units. The basic processing steps include: 1) correction for CCD detector nonlinearity; 2) dark-current correction; 3) spectral calibration; 4) radiometric calibration; 5) estimation of E_g at the time of target measurement; and optionally 6) Savitzky-Golay smoothing filtering.

The quality evaluation of unattended spectral data collected by MRI and SFLUOR box is mandatory to reject data affected by short-term changes in illumination conditions providing reliable time series. In fact, changes in illumination conditions during measurements sequences, in order to provide reliable time series. For this reason, a number of Data Quality (DQ) indices (Table 2) were defined based on two major criteria: i) stability of illumination conditions; and ii) performance of automated instrument operations (e.g. failure of the optimization algorithm). Only the data that meet the DQ indices are retained for subsequent analysis.

<Table 2>

The first data quality indicator DQ_{sza} is related to the sun position at the time of measurement, large sun zenith angles cause a significant deviation from an nominal cosine response of the up-looking foreoptic; hence, data acquired with SZA above a certain threshold (i.e. 60°) are rejected. The DQ_{sat} verifies that the collected spectra do not present saturated values. The third indicator DQ_s takes into account the stability of the down-welling irradiance measurement (E_g) during completion of an acquisition session. It is computed as the percentage of variation between the first ($Eg_{,1}$) and the second ($Eg_{,2}$) irradiance measurement. For example, if sky conditions change during a measurement session and $E_{g,2}$ is measured with cloudy conditions, the low quality of the acquisition session can be identified as an increase in the DQ index. The increase in illumination conditions during measurement of the sampled ground area (L_s) is detected by assessing the DQ_d index, computed by the ratio of L_s and E_g. Values (i.e., reflectance) larger than 100% occur when E_g is collected with partly cloudy conditions and L_s during a short clear-sky window. The DQ_l evaluates the ratio between E_g (expressed in digital counts) and DC, which represents the fraction of nominal dynamic range that can actually be used, to exclude data acquired with either too low incoming radiation or a too high DC. These conditions occur primarily at early morning or late evening (e.g. close to sunrise and sunset) or when cloudy conditions occur during the daylight hours. The DQ_h allows checking that the E_g maximum value occurs between 50% of the saturation value and saturation (maximum of the instrument dynamic range). The latter indicator is useful for excluding data collected with non-optimal values of spectrometer integration time. The *DQ* indices are then compared to their thresholds and measurements are retained if they satisfy all the *DQ* conditions. Whenever the above criteria are not met, the acquisition is rejected and no longer considered. The various thresholds presented in Table 2 were selected on the basis of theoretical and technical considerations, known deviation from true cosine response, and expert knowledge gained by analyzing in detail a number of different cases extracted from preliminary field tests.

3.2 SIF retrieval and Vegetation Indices

Once the basic processing phase is accomplished and data quality indices are evaluated, the reflectance signature is calculated. A number of spectral indices derived from incident irradiance, up-welling radiance and reflectance are calculated routinely for each acquisition. In the next sections, the photosynthetic photon flux density (PPFD), the normalized difference vegetation index (NDVI) (Rouse et al., 1973), the photochemical reflectance index (PRI) (Gamon et al., 1992), and the SIF are reported as examples. The PPFD represent the amount of down-welling radiance in the photosynthetically active radiation domain, the NDVI is a proxy of vegetation greenness, the PRI is indicative of the current de-epoxidation state of xanthophylls, and SIF is an indicator of instantaneous plant photosynthesis. The PPFD, NDVI, PRI and other vegetation indices are calculated from spectral measurements acquired with the $SPEC_{Full}$ as they do not require high spectral resolution, while SIF is derived from $SPEC_{Fluo}$ spectra. In particular, SIF is accurately computed taking advantage of more than 400 spectral bands in the oxygen absorption band at 760 nm by means of the Spectral Fitting Methods (SFM) (Meroni and Colombo, 2006; Meroni et al. 2010; Mazzoni et al. 2012).

4 Unattended field spectral measurements

The field installation of the instrument is relevant to collecting high-quality data. The nadir view is generally preferred to reduce canopy directional effects during diurnal course measurements (i.e., to minimize hot and dark spots). The set-up of the instrument foreoptic at a given height above the canopy, the dimension of the FOV and the viewing angle are key factors in collecting high quality data by reducing the directional effect associated with viewing configurations. Tripods are generally used to hold the instrument foreoptic for canopy heights below 1 m. Higher canopies have required the use of scaffolding towers or cherry-pickers to ensure a minimum distance away from the observed canopy.

The capabilities of collecting continuous and long-term spectral measurements were tested during several field campaigns promoted by ESA to support forthcoming Earth Observation missions. The first example shows the long-term measurements of vegetation optical signals and SIF during the entire vegetation growing cycle of an agricultural crop. The second example shows the collection of diurnal course measurements of TOC radiance, reflectance and SIF for different types of vegetated canopies.

4.1 Continuous and long-term measurements

In the framework of the ESA SENtinel-3 EXPeriment (SEN3EXP), the MRI was employed for long-term measurements of canopy reflectance and SIF of an alfalfa crop (*Medicago sativa L.*) located in an intensive agriculture area managed by the University of Pisa (43°40’011.04’’N; 10°18’09,90’’E). The instrument operated from June 13th 2009 (day of the year, DOY=164), until July 19th (DOY=200) for a total of 27 measurement days covering almost 2 growing cycles. The measurements were acquired with a three-minute time step roughly between 8:00 am and 4:00 pm local solar time. More than 17000 spectra were collected and covered the following phases of two consecutive growth cycles: full development, harvest, canopy growth and again full development.

The radiance spectra collected during a single acquisition session and the resulting reflectance signature collected by MRI are depicted in Figure 3. The upper panel shows the spectra collected with $SPEC_{Full}$, while the bottom panel the spectra collected with the high-resolution spectrometer $SPEC_{Fluo}$. The blue lines represent the down-welling radiance spectra (E_g/π) and the red lines correspond to up-welling canopy radiance spectra (L_s). The green lines are the apparent reflectance that show a peak at 760 nm originated by the fluorescence infilling of the O_2-A band.

<Figure 3>

The time series of hyperspectral data were filtered according to the data quality criteria, and analyzed for the retained and rejected data at the different times of the day (Figure 4). A higher number of measurements were collected near noon because the spectrometer integration time is lower, thus resulting in a shorter time required for each session. A total of 20.8% of data were rejected from the subsequent processing steps since they did not meet the data quality criteria. Most of the data were rejected due to unstable illumination conditions, while only a small percentage was rejected due to instrument failures. Occurrence of data rejection was higher in early morning and late afternoon when each acquisition session takes a longer time.

<Figure 4>

The reflectance signatures of investigated alfalfa canopy collected during the second growing cycle are shown in Figure 5. Immediately after harvesting, the canopy reflectance resembles the typical soil signature and the slight absorption in the red is due to the biomass still in the instrument FOV. Afterwards, the absorption in the red and blue increases and the reflection in the near infrared increases following the progressive growth of the crop and the consequent increase in biomass and chlorophyll content. The evolution of reflectance continues up to DOY=198, after which the reflectance signatures remain stable.

<Figure 5>

The time series of PPFD, NDVI, PRI and SIF at 760 nm derived from MRI continuous measurements were recorded and analyzed for diurnal and seasonal variability (Figure 6). The gaps in the spectral time series are due to harvesting between the two growing cycles at DOY 180. The days characterized by clear-sky conditions (e.g., DOY=164-167,197-201 etc.) show the typical diurnal evolution of the PPFD while partly cloudy or cloudy conditions (e.g. DOY=172-175) cause a more scattered pattern.

The NDVI strongly responds to vegetation growth, the values are almost constant during the beginning of measurement period when the canopy was fully developed, then they fall after harvesting (with a further reduction from DOY 184 to 186 due to progressive drying of residual biomass on the ground). After this initial phase, a rapid increase in NDVI follows the increase in crop biomass until it reaches a nearly constant value, corresponding to the maximum canopy development (full cover). Strong anisotropy effects related to sun-canopy-sensor geometry are observable in the daily courses. The maximum/minimum values of NDVI occur at larger/smaller SZAs when the direct sunlight beam enters the canopy obliquely/near vertically and therefore has the highest/lowest probability of interacting with foliage elements. The largest daily variations of NDVI are observed when canopy cover is low to intermediate (40.3%) because the variation in the gap fractions is maximum is such conditions, while at maximum canopy development the variations are limited to few percent (2.7%).

Similar to NDVI, the time evolution of PRI strongly responds to biomass presence. The daily trajectories exhibit a minimum at noon, and total variation when the crop is at its maximum development (54.0%) is greater than NDVI. This can be explained by the fact that, as mentioned before the diurnal variations of PRI are not only due to directional effects but also to variations in plant physiology.

The inter-day evolution of the SIF signal primarily responds to the amount of chlorophyll in the canopy during the different growing stages. The intra-day variation is instead modulated by photosynthetic activity that is greatest at mid-day, mainly driven by the amount of PPFD absorbed by the canopy.

The average and standard deviation values of PPFD, NDVI, PRI, and SIF were calculated at daily level (Figure 6). An average of 98 measurements are available for each day. The indices follow similar trajectories that are mostly driven by the canopy phenology. However, PRI and SIF show an additional sensitivity related to the varying environmental conditions and plant activity. For example, the average values of PPFD at DOY 168 and 172 are lower (930 μmol m^{-2} s^{-1}) than that at other days (1587 μmol m^{-2} s^{-1}). It can be observed that NDVI does not have any change for the aforementioned DOYs, while

PRI shows slightly larger values due to a minor activation of the xanthophyll cycle, and SIF has significantly low values because of the limited amount of solar irradiance. A different pattern occurs at DOY 173, which is characterized by the largest daily variations in PPFD. NDVI remains stable also in this case, whereas PRI and SIF have the largest standard deviations induced by short-term adaptation to varying solar irradiance levels. However, PRI and SIF also exhibit a different behaviors when illumination conditions are stable and canopy reaches its maximum development. In fact, PRI slightly increases during DOYs 164–167 probably due to a reduction of the xanthophyll cycle activation at the end of the phonological stage, whereas it shows a subtle decrease during DOYs 197–201 when canopy was only a few days after from its maximum development. Similarly, SIF exhibits fluctuations around the maximum level values that can be attributed to adaptation of plants related to variation of environmental variables (i.e., temperature, humidity, etc.).

<Figure 6>

The scatterplots between NDVI, PRI, and SIF (Figure 7) offer an additional indication regarding the different behaviors of the investigated variables at the seasonal level. A robust linear regressions considering deviations in both x and y variables are calculated following the method proposed in York et al., (2004); the 2σ parameters uncertainties are estimated by Monte Carlo simulations, assuming errors are Gaussian and centered. The canopy growth, and the consequent evolution of spectral variables from extremely low to maximum values, is the major driver for NDVI and PRI ($r^2_{adj} = 0.95$). This relationship is partially loss when the canopy is fully developed. On the contrary, the overall correlation between NDVI and SIF is lower ($r^2_{adj} = 0.65$) and SIF is characterized by highly variable values at full canopy development. These values, as explained before, are related to the fast response to illumination conditions or physiological processes.

<Figure 7>

4.2 Measurements on different canopies

The field surveys took place in different sites in Germany and the Czech Republic, between August and September 2012, encompassing different ecosystems. The datasets were collected on: i) a sugar beet field (50°36'54.498"N; 6°59'31.009"E) at Campus Kleinaltendorf (CKA) of the University of Bonn, Germany on August 23th; ii) a grassland field (50°52'9.90"N; 6°27'7.15"E) at Selhausen (SEL), Germany, on August 27th; and iii) a lawn carpet (49°30'7.56"N; 18°32'12.48"E) at the Bílý Kříž (BK) experimental site, Czech Republic, on September 5th.

The pictures of the three investigated canopies and the daily variations of the canopy reflectance signatures collected during field campaigns are shown in Figure 8. The varying reflectance signatures result from the different light interception, absorption and scattering processes at the different time of the day i.e. different sun-target-sensor geometry. These contributions affected the diurnal course of canopy reflectance and the derived spectral indices.

<Figure 8>

The diurnal course of PPFD, NDVI, PRI and SIF show specific vegetation features (Figure 9). The directional illumination effects observed for the reflectance signatures are partially reduced by use of two normalized vegetation indices NDVI and PRI, but slight diurnal patterns remain for the different canopies investigated (Figure 9, second and third rows). Such effects are larger for the sugar beet (Figure 9, left plots) because a greater fraction of the day was captured, the dimension of the leaves is larger, and the changes in sunlit and shadowed areas within the FOV play a stronger role during the day.

The PRI values are mostly related to the total amount of green biomass and structure: in fact, the grassland canopy, characterized by a significant fraction of yellow non-photosynthetic biomass, shows lower PRI and NDVI values than that obtained for the other two sites. The PRI diurnal courses are affected by directional effects such as the NDVI. In addition, it also depends on the activation of the xanthophyll cycle as a photo-protection mechanism during the day. The disentangling of these contributions is not trivial (Damm et al., 2015) and it is not attempted here. However, for the first time, the fact that the diurnal patterns of the different canopies show completely different behaviors (i.e., convex, concave, and nearly straight) is presented herein.

The SIF signal depends on the actual plant activity and in general, as happens for healthy canopies like that of sugar beets, it shows a diurnal course mostly driven by the incoming radiations with maximum emission around midday (Figure 9, bottom row). The diurnal course of canopies with a lower amount of green photosynthetic biomass appears to be less noticeable. For example, the SIF values measured for the grassland are lower and they remain almost constant during the day. Besides the study and interpretation of the diurnal course measurements, it is relevant to point out that the unattended and continuous data collected by MRI and SFLUOR box exhibit reliable diurnal patterns for both vegetation indices and SIF.

<Figure 9>

5 Discussion

Continuous and long-term ground-based field spectroscopy measurements represent a novel and reliable approach for understanding optical signals of the Earth’s surface. The development of instruments for collecting reliable time series involves several steps: it begins with the instrument design and proceeds through the definition of rigorous procedures for data collection, calibration, and processing. These steps are strictly interlinked and must be carefully integrated for providing high-quality data. This is particularly relevant for SIF measurements because even small errors, in both instrumental measurements and/or signal processing, can lead to significant impacts on the final retrieved values.

Therefore, we developed and integrated our customized methods and operative procedures for gaining accurate and precise observations. The dedicated software package Auto3S controls the instruments for rigorous data collection and processing. The accurate spectral and radiometric calibrations are obtained by laboratory measurements, when the instruments are not deployed in the field, and they are updated routinely by using in-field methods during long-term measurements. Finally, state-of-art algorithms (i.e. spectral fitting methods) are used for an accurate retrieval of canopy reflectance and SIF.

The field installation of the automated field spectroscopy systems is relatively easy and can be adapted to different types of agricultural and forest ecosystems. The instruments were operated in different field campaigns with the aim of studying the optical signals of different canopies and providing ground-truth measurements for the novel airborne *HyPlant* sensor. Unfortunately, SIF cannot be directly measured at canopy level even with an independent technique; therefore, the validation of SIF measurements at the top of the canopy is still an open issue for the scientific community. However, the results obtained were found to be consistent with previous studies based on similar high-resolution spectrometers (Cogliati et al., 2012; A. Damm et al., 2014; Daumard et al., 2012; Meroni et al., 2008; Rossini et al., 2010).

The continuous and long-term field spectroscopy measurements collected for the entire growth cycle of a crop show the potential of such instruments in monitoring canopy temporal evolution. Time series of NDVI, PRI, and SIF are largely sensitive to canopy biomass, chlorophyll and other chemical constituents, and 3D canopy structure. However, our results indicate that variations in PRI and SIF observed in certain conditions prove that these variables are sensitive also to dynamic and fast-response processes in plants. The short-term responses of PRI and SIF, in combination with NDVI (in general canopy reflectance), can provide novel and valuable information for improving vegetation numerical models and productivity forecast. The data collected on different types of canopy show diverse and specific patterns, which are in part caused by canopy directional effects and in part related to plant physiological response. Therefore, the interpretation of PRI and SIF in relation to plant activity must carefully involve these aspects (Damm et al., 2015) and further studies are needed to decouple the different contributions. This studies will take advantage from continuous and systematic measurements collected with instruments such as that proposed in this work.

The use of canopy radiative transfer models will be fundamental to improve the understanding of the measured signals and it may provide an essential tool for further upscaling of the signal at satellite level. In addition, the recent advances in unmanned airborne vehicles platforms and miniaturized spectrometers (Burkart et al., 2014; Zarco-Tejada et al., 2012) provide unprecedented opportunities for high-spatial, spectral and multi-angular field measurements. This novel approach, in combination with the continuous and long-term field measurements and radiative transfer models, will provide a better description of the radiative transfer of the investigated ecosystem in the spatial, spectral, temporal and angular domains. The synergy of these different measurements and radiative transfer modelling techniques will provide a robust framework for upscaling ground-based measurements towards satellite based observations.

The MRI and SFLUOR box instruments were mainly developed for vegetation studies and SIF retrieval from high-resolution data. Nevertheless, they can be used for studying temporal dynamics of other geophysical parameters. For example, Bresciani et al., (2013) employed the VNIR spectra collected by MRI to continuously monitor the chlorophyll-a concentrations in a context of inland water quality study. Moreover, the continuous measurements of down-welling irradiance could be further exploited to derive atmospheric properties. A growing number of studies estimate aerosols and trace gases by ground-based hyperspectral measurements (Dunagan et al., 2013; Hönninger et al., 2004). Beyond its relevance for the atmospheric science community, the accurate retrieval of atmospheric parameters inferred by systematic field spectroscopy measurements may also improve the operational atmospheric correction algorithms of remote sensing data.

6 Conclusions

In this paper, we presented novel automated field spectroscopy systems able to collect continuous and long-term field spectroscopy measurements. These instruments employ commercial grade optical devices available on the market with the aim of facilitating the replication of these instruments. This would promote the usage of such an instrumental concept to a wider community by providing measurements over a range of vegetation species, ecosystems, and environmental conditions. The resulting spectral library of systematic ground-based observations will provide valuable data for the interpretation of remote sensing data. The MRI and SFLUOR box instruments were mainly developed for vegetation studies and SIF retrieval from high-resolution data, exploiting almost the same retrieval concept as FLEX. The instruments and the data collection/processing methods developed allow a reliable and accurate retrieval of canopy VNIR reflectance, derived spectral indices, and SIF. The ensemble of instruments and methods developed and tested in this work can be considered a baseline for the recent attempts of ESSEM Cost Action OPTIMIZE aimed at harmonizing field optical instruments and SIF measurements.

Time series of spectral data collected during several field campaigns prove the ability of providing reliable and consistent data. Results show the overall possibility of the proposed instruments in monitoring the vegetation growth, while PRI and SIF give additional information more related to short-term variations of plant’s activity. The optical signals are strongly affected by chemical and physical characteristics of the canopy and further studies are needed to disentangle such directional effects from variations in plant activity. MRI and SFLUOR box instruments can help in these studies by providing continuous and systematic measurements. Therefore, we encourage an extensive usage of automated ground-based spectrometers and believe that the establishment of an international network involving the scientific community and space agencies will offer several benefits toward a better understanding of terrestrial ecosystems, an improvement of operational atmospheric corrections, and systematic ground-based measurements for the calibration/validation of remote sensing data and products.

Acknowledgments

The initial development and testing of MRI have been partially funded by the European Space Agency field campaigns *Sentinel-3 Experimental Campaign* in 2009 (Contract No. 22661/09/I-LG). In the framework of the ESA *HyFlex* airborne surveys to support the candidate FLEX mission (Contract No. 4000107143/12/NL/FF/If) further testing of the instrument has been implemented. We gratefully acknowledge financial support by the Transregional collaborative research centre (SFB/TR) 32 “Pattern in Soil-Vegetation-Atmosphere Systems: Monitoring, Modelling and Data assimilation” funded by the Deutsche Forschungsgemeinschaft (DFG). The authors acknowledge the funding of the CROP.SENSe.net project in the context of the Ziel 2-Programms NRW 2007–2013 “Regionale Wettbewerbsfähigkeit und Beschäftigung” by the Ministry for Innovation, Science and Research (MIWF) of the North Rhine Westphalia (NRW) state and European Union Funds for regional development (EFRE) (005-1103-0018). We are grateful to anonymous reviewers for their useful comments and suggestions.

REFERENCES

Alonso, L., Gomez-Chova, L., Vila-Frances, J., Amoros-Lopez, J., Guanter, L., Calpe, J., & Moreno, J. (2008). Improved fraunhofer line discrimination method for vegetation fluorescence quantification. *IEEE Geoscience and Remote Sensing Letters*, *5*(4), 620–624.

Baker, N. R. (2008). Chlorophyll Fluorescence: A Probe of Photosynthesis In Vivo. *Annual Review of Plant Biology*, *59*(1), 89–113. doi:10.1146/annurev.arplant.59.032607.092759

Balzarolo, M., Anderson, K., Nichol, C., Rossini, M., Vescovo, L., Arriga, N., … Martín, M. P. (2011). Ground-based optical measurements at European flux sites: A review of methods, instruments and current controversies. *Sensors*, *11*(8), 7954–7981. doi:10.3390/s11087954

Berk, A., Anderson, G. P., Acharya, P. K., Bernstein, L. S., Muratov, L., Lee, J., … Shettle, E. P. (2006). MODTRAN5: 2006 update. In *Proceedings of SPIE - The International Society for Optical Engineering* (Vol. 6233 II).

Corp, L. A., Cook, B. D., Middleton, E. M., Cheng, Y.-B., Huemmrich, K. F., & Campbell, P. K. E. (2010). Fusion: A f□ully u□ltraportable s□ystem for i□maging o□bjects in n□ature. In *2010 IEEE International Geoscience and Remote Sensing Symposium* (pp. 1671–1674). IEEE. doi:10.1109/IGARSS.2010.5652788

Damm, A., Erler, A., Hillen, W., Meroni, M., Schaepman, M. E., Verhoef, W., & Rascher, U. (2011). Modeling the impact of spectral sensor configurations on the FLD retrieval accuracy of sun-induced chlorophyll fluorescence. *Remote Sensing of Environment*, *115*(8), 1882–1892. doi:10.1016/j.rse.2011.03.011

Damm, A., Guanter, L., Verhoef, W., Schläpfer, D., Garbari, S., & Schaepman, M. E. (2015). Impact of varying irradiance on vegetation indices and chlorophyll fluorescence derived from spectroscopy data. *Remote Sensing of Environment*, *156*, 202–215. doi:10.1016/j.rse.2014.09.031

Damm, A., Kneubuhler, M., Schaepman, M. E., & Rascher, U. (2012). Evaluation of gross primary production (GPP) variability over several ecosystems in Switzerland using sun-induced chlorophyll fluorescence derived from APEX data. In *2012 IEEE International Geoscience and Remote Sensing Symposium* (pp. 7133–7136). IEEE. doi:10.1109/IGARSS.2012.6352018

Daumard, F., Champagne, S., Fournier, A., Goulas, Y., Ounis, A., Hanocq, J.-F., & Moya, I. (2010). A field platform for continuous measurement of canopy fluorescence. *IEEE Transactions on Geoscience and Remote Sensing*, *48*(9), 3358–3368.

Drolet, G., Wade, T., Nichol, C. J., MacLellan, C., Levula, J., Porcar-Castell, A., … Vesala, T. (2014). A temperature-controlled spectrometer system for continuous and unattended measurements of canopy spectral radiance and reflectance. *International Journal of Remote Sensing*, *35*(5), 1769–1785. doi:10.1080/01431161.2014.882035

Drusch, M., Moreno, J., Goulas, Y., F., M., North, P., & Rascher, U. (2008). Candidate Earth Explorer Core Mission - FLEX - FLEXuorescence Explorer - Report for Assessment. *ESA Comunication Production Office*, *ISBN: 987*-(SP-1313/4).

Flexas, J., Escalona, J. M., Evain, S., Gulías, J., Moya, I., Osmond, C. B., & Medrano, H. (2002). Steady-state chlorophyll fluorescence (Fs) measurements as a tool to follow variations of net CO2 assimilation and stomatal conductance during water-stress in C3 plants. *Physiologia Plantarum*, *114*(2), 231–240. doi:10.1034/j.1399-3054.2002.1140209.x

Galeazzi, C., Varacalli, G., Longo, F., Lopinto, E., Garramone, L., And, & Capentiero, R. (2009). Overview of the PRISMA mission. In *Proc. 6th EARSeL SIG Workshop on Imaging Spectroscopy*. Tel Aviv, Israel.

Gamon, J. A., Cheng, Y., Claudio, H., MacKinney, L., & Sims, D. A. (2006). A mobile tram system for systematic sampling of ecosystem optical properties. *Remote Sensing of Environment*, *103*(3), 246–254. doi:http://dx.doi.org/10.1016/j.rse.2006.04.006

Gamon, J. A., Peñuelas, J., & Field, C. B. (1992). A narrow-waveband spectral index that tracks diurnal changes in photosynthetic efficiency. *Remote Sensing of Environment*, *41*(1), 35–44. doi:http://dx.doi.org/10.1016/0034-4257(92)90059-S

Gamon, J. A., Rahman, A. F., Dungan, J. L., Schildhauer, M., & Huemmrich, K. F. (2006). Spectral Network (SpecNet)—What is it and why do we need it? *Remote Sensing of Environment*, *103*(3), 227–235. doi:http://dx.doi.org/10.1016/j.rse.2006.04.003

Gao, B.-C., Montes, M. J., & Davis, C. O. (2004). Refinement of wavelength calibrations of hyperspectral imaging data using a spectrum-matching technique. *Remote Sensing of Environment*, *90*(4), 424–433. doi:http://dx.doi.org/10.1016/j.rse.2003.09.002

Goetz, A. F. H. (2009). Three decades of hyperspectral remote sensing of the Earth: A personal view. *Remote Sensing of Environment*, *113, Suppl*(0), S5 – S16. doi:http://dx.doi.org/10.1016/j.rse.2007.12.014

Green, R. O., Asner, G., Ungar, S., & Knox, R. (2008). NASA Mission to Measure Global Plant Physiology and Functional Types. In *Aerospace Conference, 2008 IEEE* (pp. 1–7). doi:10.1109/AERO.2008.4526244

Guanter, L., Richter, R., & Moreno, J. (2006). Spectral calibration of hyperspectral imagery using atmospheric absorption features. *Applied Optics*, *45*(10), 2360–2370.

Guanter, L., Segl, K., Sang, B., Alonso, L., Kaufmann, H., & Moreno, J. (2009). Scene-based spectral calibration assessment of high spectral resolution imaging spectrometers. *Optics Express*, *17*(14), 11594–11606.

Hilker, T., Nesic, Z., Coops, N. C., & Lessard, D. (2010). A new, automated, multiangular radiometer instrument for tower-based observations of canopy reflectance (AMSPEC II). *Instrumentation Science and Technology*, *38*(5), 319–340.

Huber, S., Tagesson, T., & Fensholt, R. (2014). An automated field spectrometer system for studying VIS, NIR and SWIR anisotropy for semi-arid savanna. *Remote Sensing of Environment*, *152*, 547–556. doi:10.1016/j.rse.2014.06.007

Kaufmann, H., Segl, K., Guanter, L., Hofer, S., Foerster, K.-P., Stuffler, T., … Chlebek, C. (2008). Environmental mapping and analysis program (ENMAP) - recent advances and status. In *International Geoscience and Remote Sensing Symposium (IGARSS)* (Vol. 4, pp. IV109–IV112).

Kraft, S. (2012). *Technical note on Update of FLORIS SNR model - IPD-TN-ESA-313* (No. IPD-TN-ESA-313).

Kraft, S., Bezy, J.-L., Del Bello, U., Berlich, R., Drusch, M., Franco, R., … Silvestrin, P. (2013). FLORIS: Phase a status of the fluorescence imaging spectrometer of the earth explorer mission Candidate FLEX. In *Proceedings of SPIE - The International Society for Optical Engineering* (Vol. 8889).

Leuning, R., Hughes, D., Daniel, P., Coops, N. C., & Newnham, G. (2006). A multi-angle spectrometer for automatic measurement of plant canopy reflectance spectra. *Remote Sensing of Environment*, *103*(3), 236–245. doi:http://dx.doi.org/10.1016/j.rse.2005.06.016

Mazzoni, M., Meroni, M., Fortunato, C., Colombo, R., & Verhoef, W. (2012). Retrieval of maize canopy fluorescence and reflectance by spectral fitting in the O 2-A absorption band. *Remote Sensing of Environment*, *124*, 72–82. doi:10.1016/j.rse.2012.04.025

Meroni, M., Barducci, A., Cogliati, S., Castagnoli, F., Rossini, M., Busetto, L., … Di Cella, U. M. (2011). The hyperspectral irradiometer, a new instrument for long-term and unattended field spectroscopy measurements. *The Review of scientific instruments*, *82*(4), 043106. doi:10.1063/1.3574360

Meroni, M., Busetto, L., Colombo, R., Guanter, L., Moreno, J., & Verhoef, W. (2010). Performance of Spectral Fitting Methods for vegetation fluorescence quantification. *Remote Sensing of Environment*, *114*(2), 363–374. doi:http://dx.doi.org/10.1016/j.rse.2009.09.010

Meroni, M., Busetto, L., Guanter, L., Cogliati, S., Crosta, G. F., Migliavacca, M., … Colombo, R. (2010). Characterization of fine resolution field spectrometers using solar Fraunhofer lines and atmospheric absorption features. *Applied optics*, *49*(15), 2858–2871. doi:10.1364/AO.49.002858

Meroni, M., & Colombo, R. (2006). Leaf level detection of solar induced chlorophyll fluorescence by means of a subnanometer resolution spectroradiometer. *Remote Sensing of Environment*, *103*(4), 438–448. doi:http://dx.doi.org/10.1016/j.rse.2006.03.016

Meroni, M., & Colombo, R. (2009). 3S: A novel program for field spectroscopy. *Computers and Geosciences*, *35*(7), 1491–1496.

Meroni, M., Rossini, M., Picchi, V., Panigada, C., Cogliati, S., Nali, C., & Colombo, R. (2008). Assessing steady-state fluorescence and PRI from hyperspectral proximal sensing as early indicators of plant stress: The case of ozone exposure. *Sensors*, *8*(3), 1740–1754. doi:10.3390/s8031740

Middleton, E. M., Ungar, S. G., Mandl, D. J., Ong, L., Frye, S. W., Campbell, P. E., … Pollack, N. H. (2013). The Earth Observing One (EO-1) Satellite Mission: Over a Decade in Space. *Selected Topics in Applied Earth Observations and Remote Sensing, IEEE Journal of*, *6*(2), 243–256. doi:10.1109/JSTARS.2013.2249496

Papageorgiou, G. C., & Govindjee. (2004). Chlorophyll a fluorescence: a signature of photosynthesis. *Advances in Photosynthesis and Respiration*, *19*.

Rossini, M., Nedbal, L., Guanter, L., Ač, A., Alonso, L., Burkart, A., … Rascher, U. (2015). Red and far-red sun-induced chlorophyll fluorescence as a measure of plant photosynthesis. *Geophysical Research Letters*, n/a–n/a. doi:10.1002/2014GL062943

Rouse, J. W., Haas, R. H., Schell, J. A., & Deering, D. W. (1973). Monitoring Vegetation Systems in the Great Plains with ERTS. In *Third ERTS Symposium, NASA SP-353, vol. 1, US Government Printing Office, Washington DC, 309–317, 1973*.

Schaepman, M. E., Ustin, S. L., Plaza, A. J., Painter, T. H., Verrelst, J., & Liang, S. (2009). Earth system science related imaging spectroscopy—An assessment. *Remote Sensing of Environment*, *113*, S123–S137. doi:10.1016/j.rse.2009.03.001

Schaepman-Strub, G., Schaepman, M. E., Painter, T. H., Dangel, S., & Martonchik, J. V. (2006). Reflectance quantities in optical remote sensing—definitions and case studies. *Remote Sensing of Environment*, *103*(1), 27–42. doi:http://dx.doi.org/10.1016/j.rse.2006.03.002

Ungar, S. G., Pearlman, J. S., Mendenhall, J. A., & Reuter, D. (2003). Overview of the Earth Observing One (EO-1) mission. *Geoscience and Remote Sensing, IEEE Transactions on*, *41*(6), 1149–1159. doi:10.1109/TGRS.2003.815999

York, D., Evensen, N. M., Martínez, M. L., & De Basabe Delgado, J. (2004). Unified equations for the slope, intercept, and standard errors of the best straight line. *American Journal of Physics*, *72*(3), 367. doi:10.1119/1.1632486

Zarco-Tejada, P. J., Berni, J. A. J., Suárez, L., Sepulcre-Cantó, G., Morales, F., & Miller, J. R. (2009). Imaging chlorophyll fluorescence with an airborne narrow-band multispectral camera for vegetation stress detection. *Remote Sensing of Environment*, *113*(6), 1262–1275.

Zarco-Tejada, P. J., Catalina, A., González, M. R., & Martín, P. (2013). Relationships between net photosynthesis and steady-state chlorophyll fluorescence retrieved from airborne hyperspectral imagery. *Remote Sensing of Environment*, *136*, 247–258.

Figure captions

Figure 1: A) Schematic drawing of the automated field spectroradiometers (not in scale). (1) cosine-response entrance foreoptics points to Zenit to collect E_g; (2) bare fiber optic collects the up-welling radiance L_s from the target; (3) optical multiplexer is housed inside the protective box; (4) High Resolution HR4000 spectrometers: (4a) $SPEC_{Full}$ (400-1000 nm), (4b) $SPEC_{Fluo}$ (700-800 nm); (5) controller PC; (6) cooling system; B) typical field installation of MRI; C) the SFLUOR box operated on top of a tower.

Figure 2: Flow-chart of the data collection routines implemented in the Auto3S software to collect a single measurement session by using the single-channel (left) and dual-channel (right) optimization methods.

Figure 3: Spectra collected throughout a single acquisition session over a vegetated surface: down-welling radiance E_g/π (blue line), up-welling radiances L_s (red line) and the resulting apparent reflectance ρ^* (green line) for the $SPEC_{Full}$ (upper plot) and $SPEC_{Fluo}$ (lower plot). The reflectance peak at 760 nm visible in the $SPEC_{Fluo}$ data is originated by the fluorescence infilling at the O_2-A band.

Figure 4: Occurrence of data rejection in the time series recorded during the SEN3EXP field campaign at the alfalfa measurement site. The number of spectra collected at different times of the day are indicated by the vertical bars distributed as retained (gray color) and rejected (black color) data. The black line shows the percentage of data rejected.

Figure 5: Time evolution of the apparent reflectance signature from harvested canopy (i.e. almost bare soil) to fully developed canopy of the investigated alfalfa crop, from DOY=186 to DOY=198 with a three-day time step.

Figure 6: Time series of Photosynthetic Photon Flux Density (PPFD), Normalized Difference Vegetation Index (NDVI), Photochemical Reflectance Index (PRI) and Sun-Induced Chlorophyll Fluorescence at 760 nm (SIF) collected over an alfalfa field during the SEN3EXP campaign. The small dots represent the continuous measurements, squares (scaled for clarity) and error bars represent are daily average and standard deviations.

Figure 7: Scatterplots between daily average values of NDVI, PRI (left) and SIF (right) during the entire growing season. The linear regression (solid line) and relative uncertainties (dashed line) are shown in red.

Figure 8: The RGB pictures (upper plot) of the sugar beet, grassland and lawn carpet canopies measured respectively during field surveys: i) Campus Kleinaltendorf (left plot); ii) Selhausen (middle plot); iii) Bílý Kříž (right plot) are shown in the upper plots. The daily course of apparent canopy reflectance signatures at the different times of the day (expressed as fraction of the day) are shown in the lower plots.

Figure 9: Measurements of daily courses of PPFD, NDVI, PRI and fluorescence at 760 nm collected on three different types of canopy. From left to right measurements on: i) sugar beet field Campus Kleinaltendorf (KA); ii) grassland field Selhausen (SEL); iii) lawn carpet in Bílý Kříž (BK).

Table 1: Characteristics of the High-Resolution HR4000 spectrometers; FWHM indicates the average band width in the covered spectral range, the Spectral Sampling Interval (SSI) refers to the distance between adjacent spectral bands.

ID	Range (nm)	FWHM (nm)	SSI (nm)
$SPEC_{Full}$	400-1000	1.0	0.25
$SPEC_{Fluo}$	700-800	0.1	0.10

Table 2: Data Quality indexes developed to select and filter poor-quality data. Threshold is the criteria for which data are rejected.

Label	***Description***	***Computation***	***Threshold***
DQ_{sza}	solar zenith angle		<60°
DQ_{sat}	spectrum saturation	counts < sv	0
DQ_{s}	E_g stability	$\lvert E_{g,1}- E_{g,2}\rvert*100/ E_{g,1}$	<10%
DQ_{d}	E_g vs. L_s stability	$\pi L_s/E_g*100$	>100%
DQ_{l}	optimization lower limit	E_g (counts)/ DC*100	>30%
DQ_{h}	optimization higher limit	max E_g > 0.5 sv	1

Figure 1

Click here to download Figure: figure1.eps

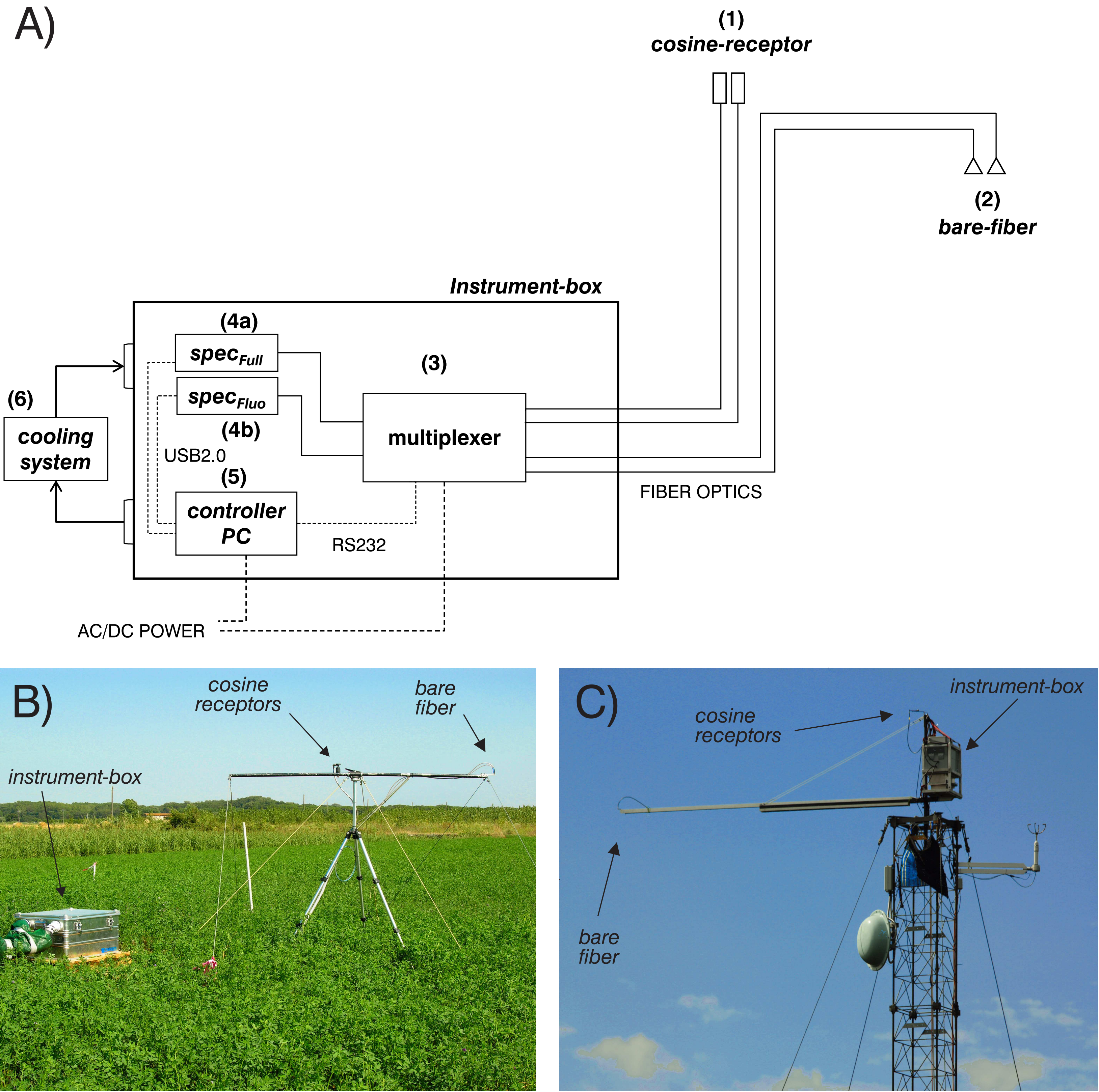

Figure 2

Click here to download Figure: figure2.eps

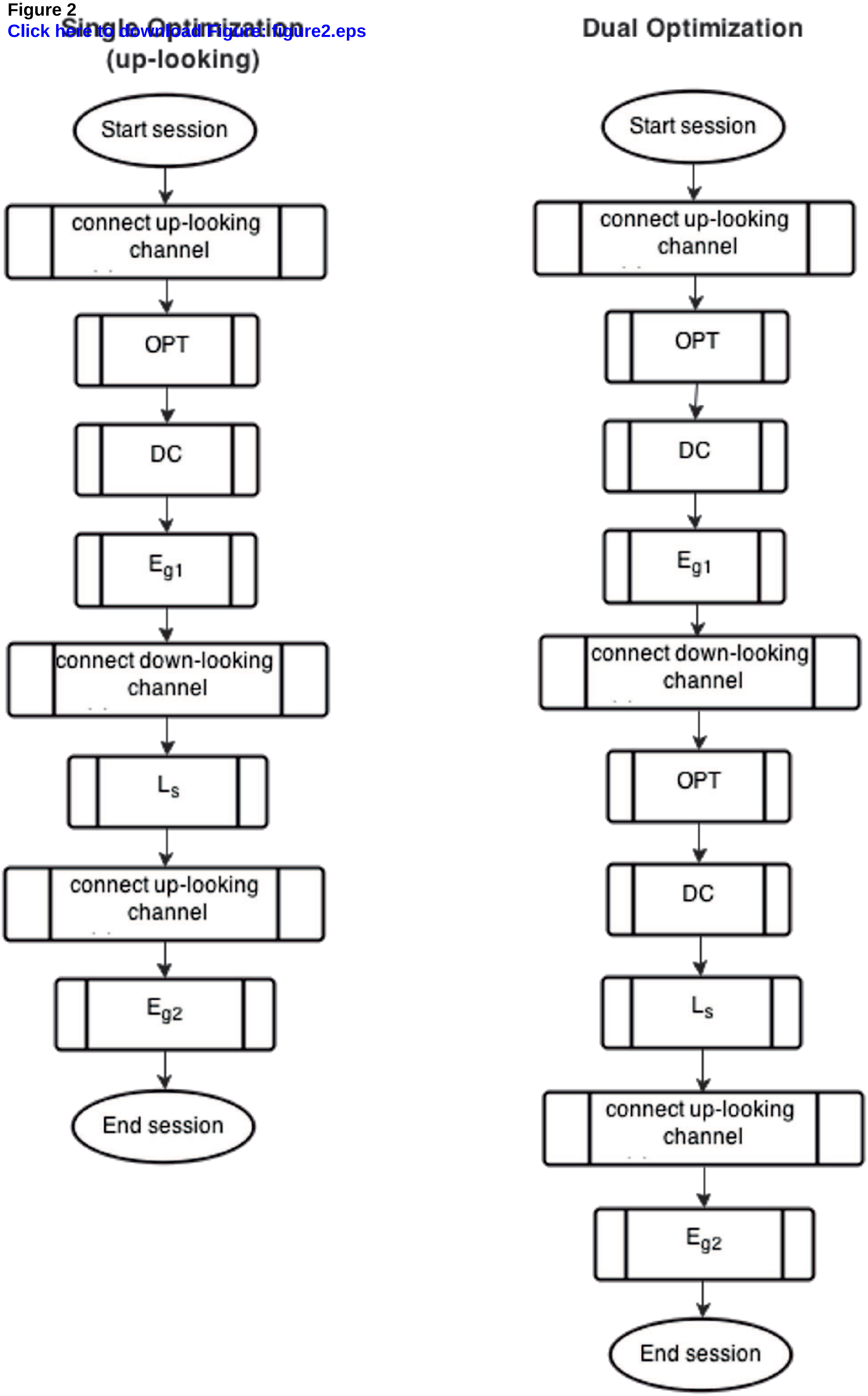

Figure 3
Click here to download high resolution image

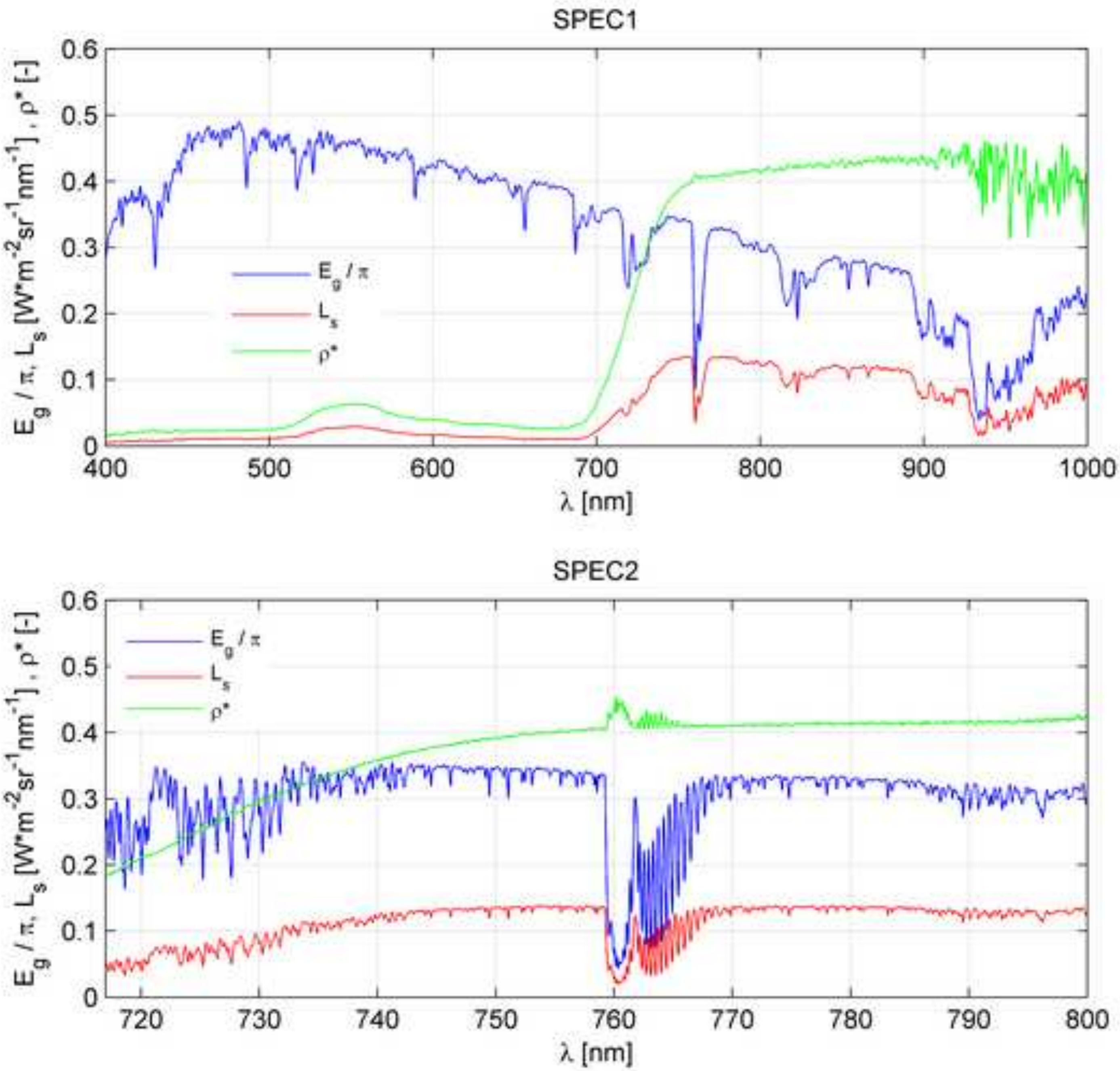

Figure 4
Click here to download high resolution image

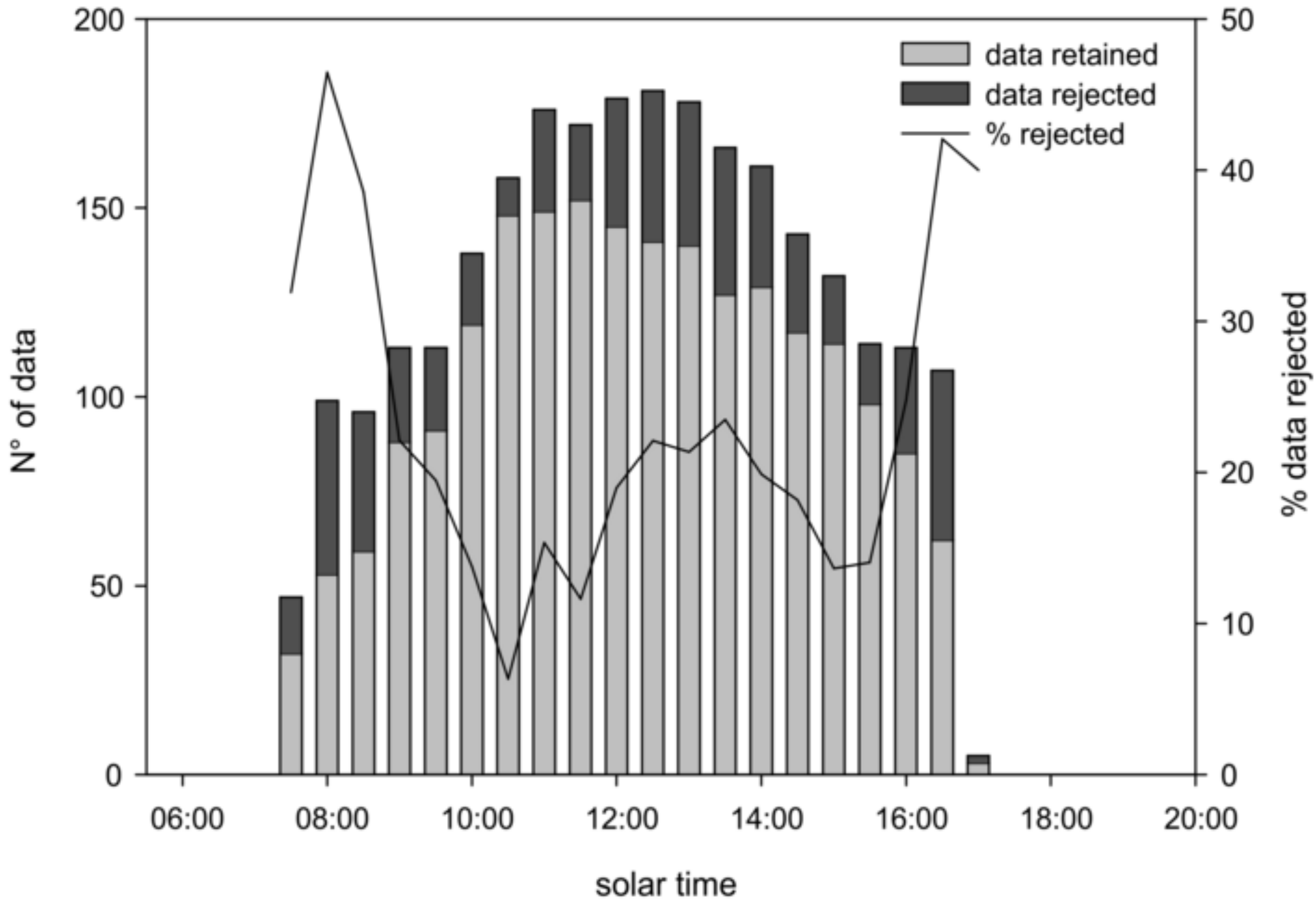

Figure 5
Click here to download high resolution image

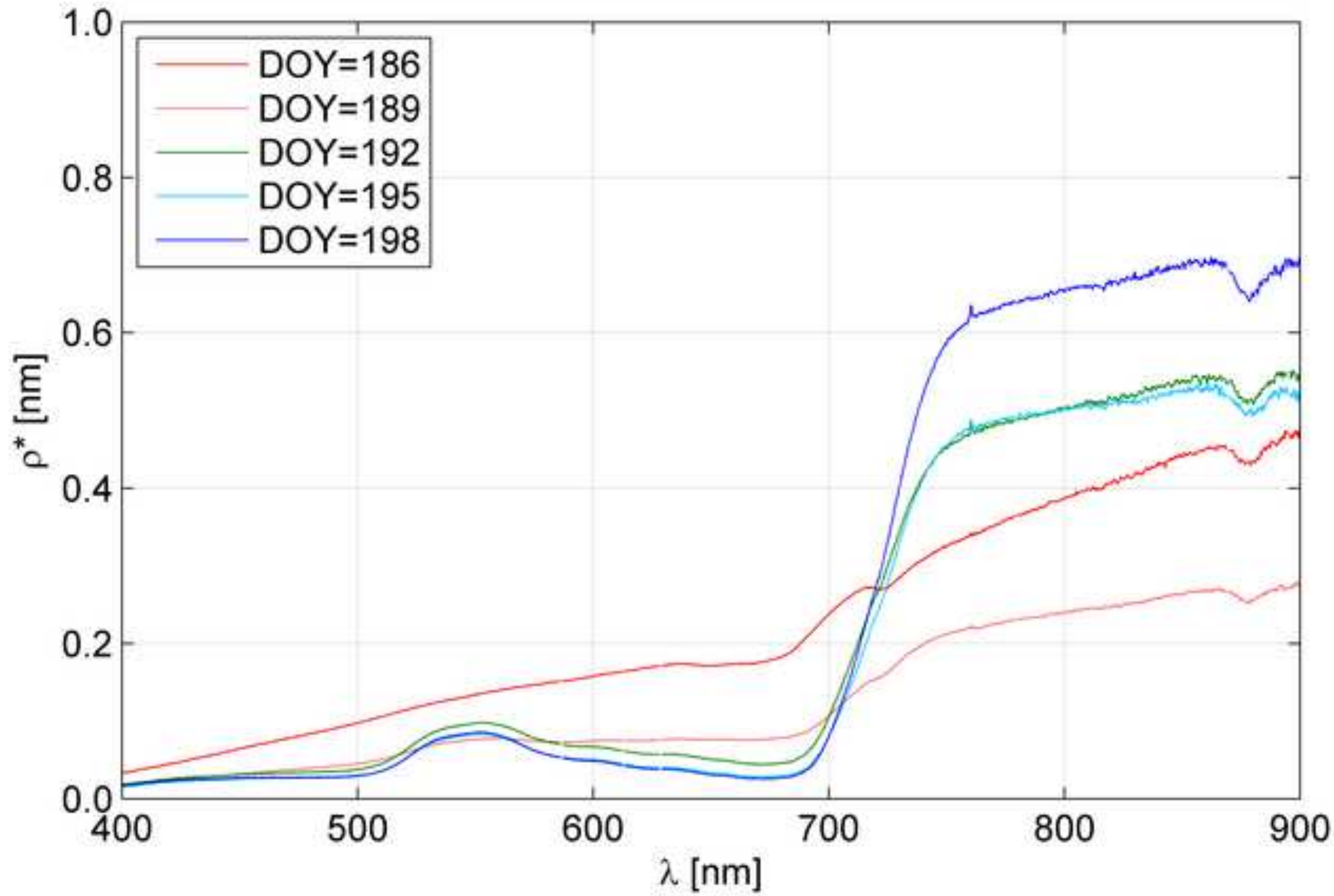

Figure 6

Click here to download high resolution image

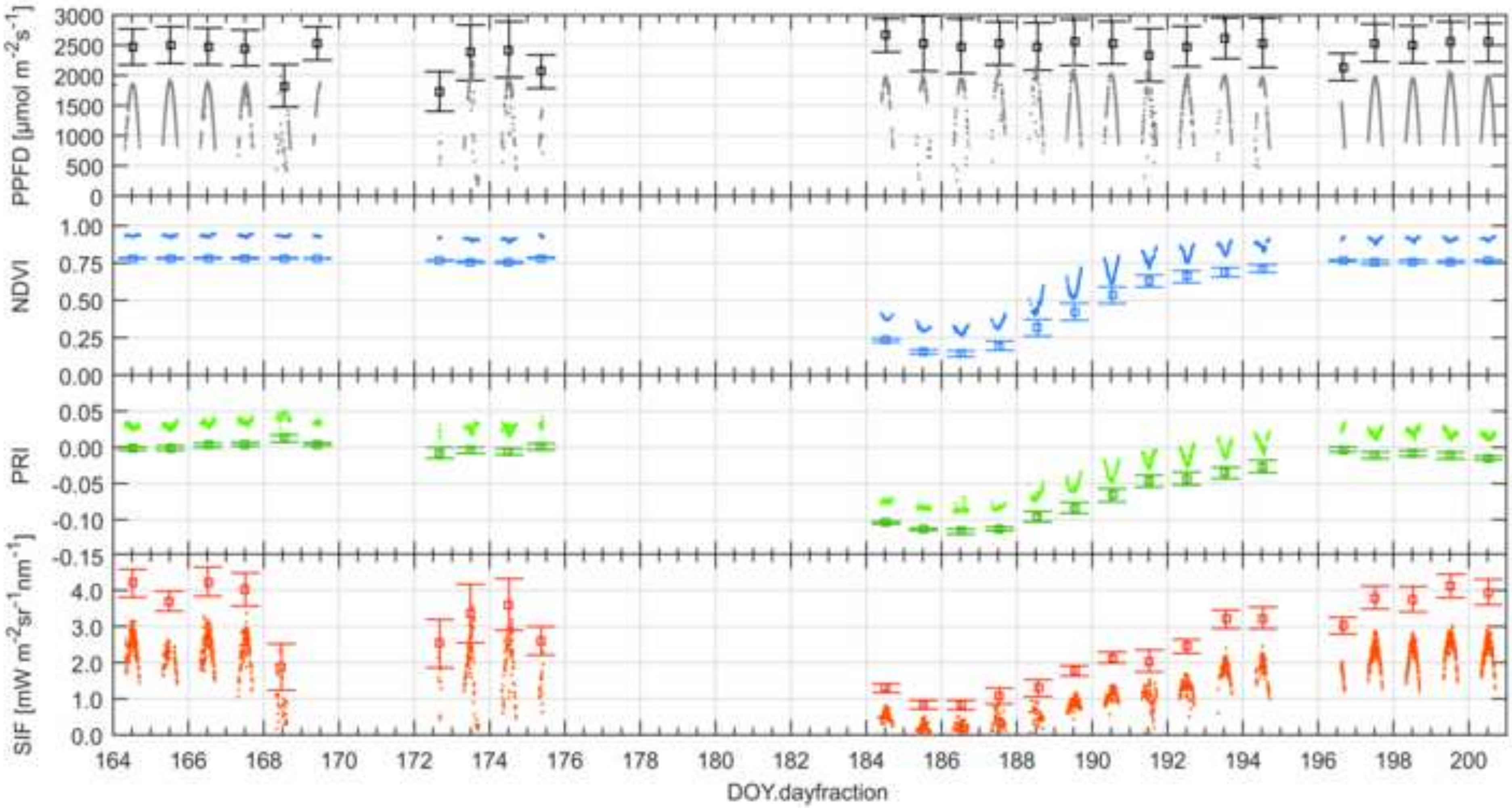

Figure 7
Click here to download high resolution image

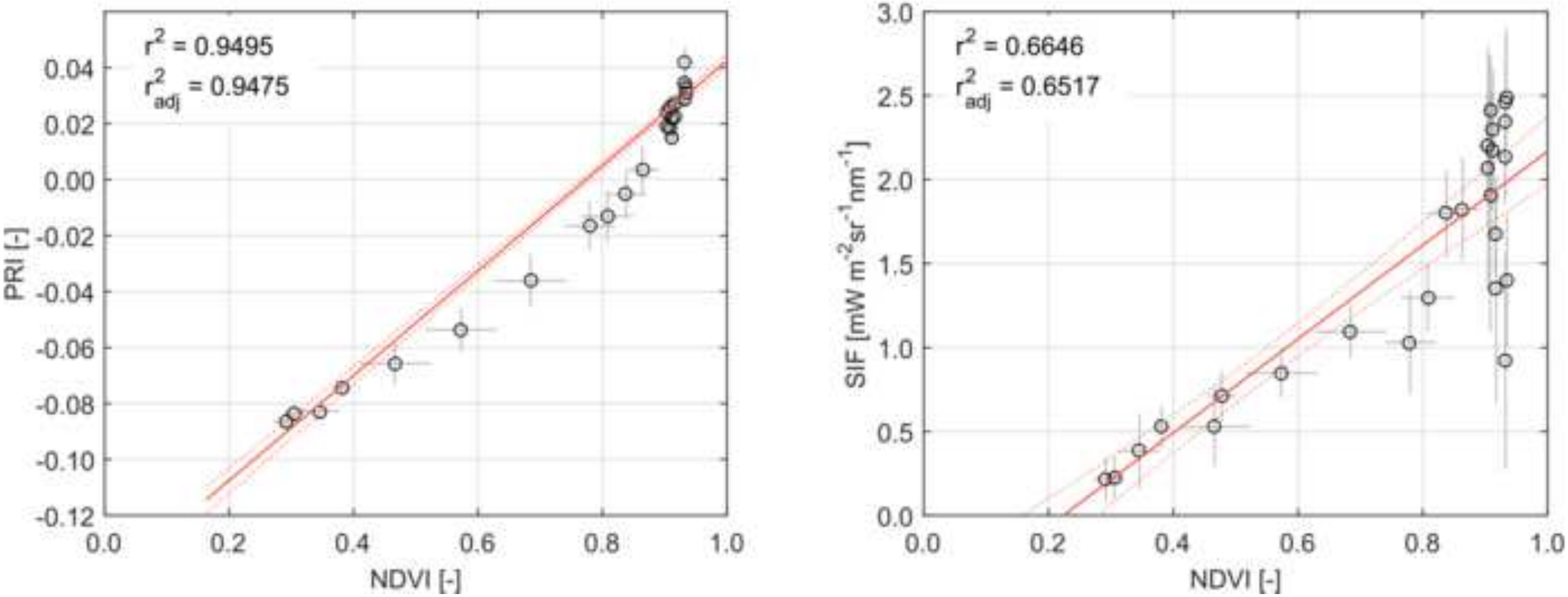

Figure 8
Click here to download high resolution image

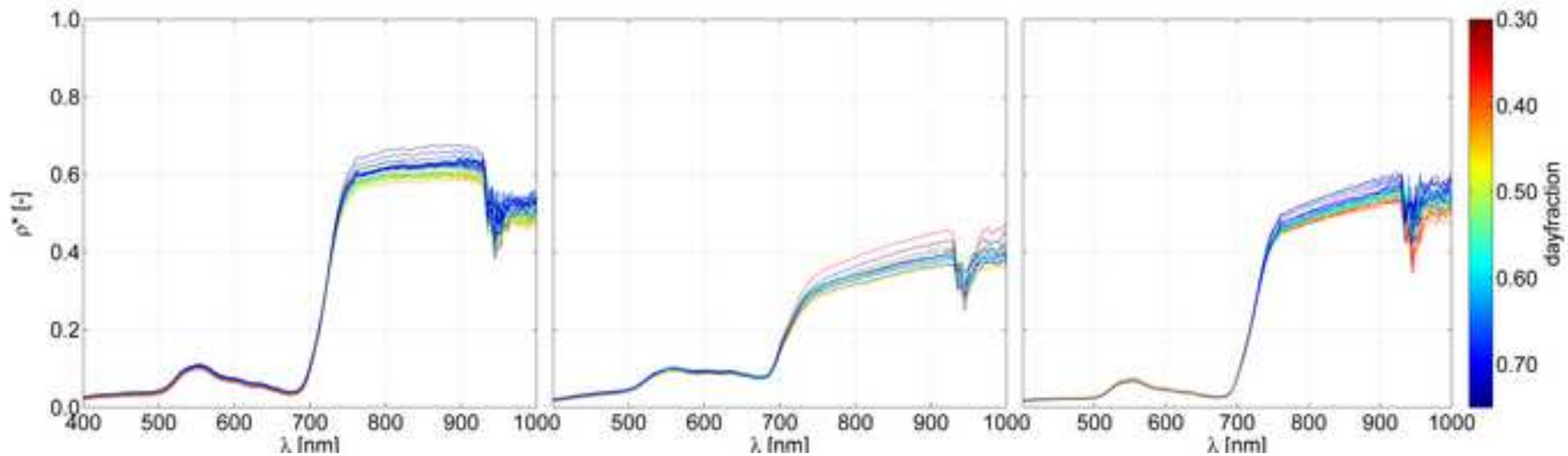

Figure 9
Click here to download high resolution image